

Temperature monitoring and lesion volume estimation during double-applicator laser-induced thermotherapy in ex vivo swine pancreas: a preliminary study

Paola Saccomandi · Emiliano Schena · Francesco Giurazza · Riccardo Del Vescovo · Michele A. Caponero · Luca Mortato · Francesco Panzera · Roberto L. Cazzato · Francesco R. Grasso · Francesco M. Di Matteo · Sergio Silvestri · Bruno B. Zobel

Received: 27 November 2012 / Accepted: 28 May 2013 / Published online: 19 June 2013
© Springer-Verlag London 2013

Abstract Tissue temperature distribution plays a crucial role in the outcome of laser-induced thermotherapy (LITT), a technique employed for neoplasias removal. Since recent studies proposed LITT for pancreatic tumors treatment, assessment of temperature and of its effects around the laser applicator could be useful to define optimal laser settings. The aims of this work are temperature monitoring and measurement of ablated tissue volume in an ex vivo porcine pancreas undergoing double-applicator LITT. A three-dimensional numerical model is implemented to predict temperature rise and volumes of ablated tissue in treated pancreas. Experiments are performed to validate the model, with two modalities: (1) 12-fiber Bragg grating sensors are adopted to monitor the heating and cooling during LITT at several distances from the applicators tip, and (2) 1.5-T MR imaging is used to estimate the ablated volume. Experimental data agree with theoretical ones: at 2 mm from both applicator tips, the maximum temperature increase is approximately

60 °C downward from the tips, while it increases of about 40 °C and 30 °C, respectively, at the level and upward from the tips. This behavior occurs also at other distances, proving that the tissue downward from the tip is mostly heated. Furthermore, the estimated volume with MRI agrees with theoretical one (i.d., 0.91 ± 0.09 vs. 0.95 cm^3). The encouraging results indicate that the model could be a suitable tool to choose the optimal laser settings, in order to control the volume of ablated tissue.

Keywords Laser-induced thermotherapy · Pancreas cancer · Laser–tissue interaction · Fiber optic sensors

Introduction

Laser-induced interstitial thermotherapy (LITT) is a minimally invasive surgical procedure used to treat neoplasia of several organs, such as the brain, liver, and kidneys. Laser radiation is guided within a fiber-optic applicator, with the tip placed in contact with the tumoral region requiring treatment. The therapy is based on the photothermal effects related to the transformation of the absorbed light energy into heat, which results in tissue hyperthermia around the applicator [1]. The optimal outcome for LITT is determined by the complete and controlled removal of the tumor volume and the absence of thermal damage to healthy surrounding tissue. The removal of tissue mass is due to several mechanisms, such as plasma formation, tissue vaporization, combustion, and explosive tissue fragmentation.

Since the amount of tissue being damaged and ablated is related to the heating and the history of the heating, the tissue temperature is a crucial parameter to be taken into account during the procedure [2].

P. Saccomandi · E. Schena (✉) · S. Silvestri
Unit of Measurements and Biomedical Instrumentation,
Università Campus Bio-Medico di Roma, Rome, Italy
e-mail: e.schena@unicampus.it

F. Giurazza · R. Del Vescovo · L. Mortato · R. L. Cazzato ·
F. R. Grasso · B. B. Zobel
Radiology Department, Università Campus Bio-Medico di Roma,
Rome, Italy

M. A. Caponero
Photonics Micro- and Nano-structures Laboratory,
Research Centre of Frascati, ENEA, Frascati, Italy

F. Panzera · F. M. Di Matteo
Endoscopy Department, Università Campus Bio-Medico di Roma,
Via Álvaro del Portillo, 200,
00128 Rome, Italy

Recently, researchers have been working to introduce LITT in the treatment of pancreatic cancer [3]. In medical practice, the management of pancreatic cancer is a big effort for clinicians because only 20 % of patients are surgical candidates at the time of the diagnosis, limited solutions can be adopted for unresectable cancer, and because of its high mortality and morbidity [4]. Furthermore, the procedure used to surgically resect the neoplasia, known as the “Whipple procedure,” is a complex and lengthy operation, strongly dependent on the surgeon, and requires a long and difficult recovery [5]. These issues encourage research regarding the introduction of new solutions in pancreatic cancer management. LITT could improve the outcome of pancreatic cancer management by introducing some advantages, such as minimal invasiveness, the ability to treat inoperable patients, and a reduction in operating time by tens of minutes.

Recently, LITT outcomes on ex vivo pancreas have been investigated in terms of the temperature distribution around a single applicator and of the ablated and damaged tissue volume [6]. Results achieved in this previous study encouraged us to further examine LITT effects on the pancreas by adopting a different technical solution. The main novelty introduced in this work is the placement of two fiber-optic applicators inside an ex vivo healthy porcine pancreas during LITT. Numerical simulations based on Pennes' model [7] have provided promising outcomes about temperature maps and size of ablated tissue volumes caused by the interaction between radiation delivered by the two applicators and the pancreas. Experimental trials have been subsequently performed by splitting Nd:YAG laser radiation within the two applicators that deliver the same power. The effects of the procedure on the pancreas are assessed in two modalities: (1) the temperature distribution is monitored by means of 12 fiber Bragg grating sensors placed inside the tissue both during LITT, to describe the heating, and after the laser treatment is stopped, to describe the cooling phenomenon; (2) the shape and size of the ablated tissue volume are measured on the pancreas after treatment. Estimation of the ablated tissue volume is performed by MR images of the treated pancreas.

Materials and methods

A continuous-wave radiation ($\lambda=1,064$ nm), emitted by means of a Nd:YAG laser, is conveyed within two bare fiber optic applicators consisting of a quartz optical fiber with a 300- μm core diameter. LITT has been performed by Nd:YAG laser because it emits at λ contained into the “therapeutic window” (i.e., from 600 to 1,200 nm [8]). The tips of the two applicators are placed parallel to each other inside the ex vivo healthy porcine pancreas, at a distance of 4 mm between their centers (Fig. 1a, b).

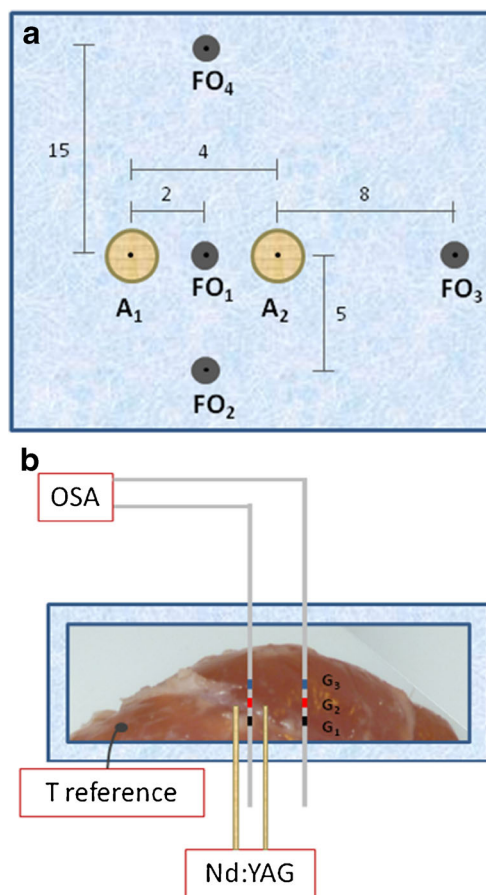


Fig. 1 Schematic representation of the relative position between the two applicators A_1 and A_2 and the fiber where the FBG sensors are mounted. **a** Top view: configuration and relative distances (expressed in millimeters) among A_1 , A_2 , and the four temperature sensors S_1 , S_2 , S_3 , and S_4 . **b** Position of the three FBG mounted on each fiber: one is positioned 2 mm upward from applicators tip (black), one is aligned with tips (red), and one is placed 2 mm downward from the tips (blue). The temperature sensor used as a reference is also shown

The effects of the laser–tissue interaction are investigated with two aims: (1) a theoretical model is developed in order to predict the temperature distribution around the applicators during the procedure and the lesion volume caused by hyperthermia; (2) experiments are performed to monitor the temperature rise during LITT, to estimate the ablated tissue volume and to validate the theoretical model. In both numerical simulations and experiments, a typical laser setting [9] is considered: laser power (P) of 3 W for each applicator, laser energy (E) of 1,500 J, and treatment time (t_L) of 500 s. Theoretical and experimental temperature trends are represented for 1,800 s (the 500 s during treatment and the subsequent 1,300 s showing tissue cooling).

The methods employed to achieve the theoretical prediction and the materials used to accomplish the experimental assessment will be described in detail in the following subsections.

Theoretical model

As described in a previous study [6], the laser beam irradiance, $I(x,y)$ (watts per square meter), is modeled using a 2D Gaussian distribution with the standard deviation σ equal to $r_f/3$ (where r_f is the radius of the two applicators core) in order to obtain 99 % of P contained within the fiber core [10]:

$$I(x,y) = I_0 \cdot e^{-\frac{x^2+y^2}{2\sigma^2}} \quad (1)$$

where $I_0 = \frac{P}{2 \cdot \pi \cdot \sigma^2}$ is the collimated irradiance (watts per square meter). Lambert–Beer's law is used to express the relation between the laser heat source term Q_1 (watts per cubic meter) and the tissue optical properties:

$$Q_1 = \mu_{\text{eff}} \cdot I(x,y) \cdot e^{-\mu_{\text{eff}} \cdot z} \quad (2)$$

Scattering and absorption phenomena in the tissue are modeled by the effective attenuation coefficient μ_{eff} (per meter), which depends on the absorption coefficient μ_a (per meter), the scattering coefficient μ_s (per meter), and the anisotropy coefficient g :

$$\mu_{\text{eff}} = \sqrt{3\mu_a(\mu_a + \mu_s(1-g))} \quad (3)$$

μ_{eff} determines the amount of laser light penetrating into the tissue, and therefore, the amount of laser energy converted into heat.

The thermal response of the pancreas is related to the P deposition in tissue and is theoretically predicted by the Pennes' bioheat equation [7], without considering the metabolic heat generation and the heat contribution due to blood perfusion because ex vivo pancreases are treated:

$$\rho \cdot c \frac{\partial T(x,y,z,t)}{\partial t} = \nabla(k \nabla T(x,y,z,t)) + Q_1 - Q_e \quad (4)$$

where ρ is the tissue density (kilograms per cubic meter), c is the tissue specific heat (joules per kilogram per kelvin), and k is the tissue heat conductivity (watts per meter per kelvin). $T(x,y,z,t)$ is the tissue temperature, expressed as a function of spatial coordinates x , y , and z , and of time, t (seconds). The tissue is assumed to be homogeneous and isotropic to make the heat transfer analysis more feasible and to maintain generality. Q_e (watts per cubic meter) is the power absorption due to water evaporation [11]:

$$Q_e = -\lambda \cdot \frac{d\rho_w}{dt} \quad (5)$$

where λ is the water's latent heat (joules per kilogram), and ρ_w is the water density (kilograms per cubic meter) that depends on T :

$$\rho_w(T) = \begin{cases} 0.778 \cdot \left(1 - e^{\frac{T-106}{3.42}}\right) & T \leq 103 \text{ } ^\circ\text{C} \\ 0.0289 \cdot T^3 - 8.924 \cdot T^2 + 919.6 \cdot T - 31573 & 103 \text{ } ^\circ\text{C} < T < 104 \text{ } ^\circ\text{C} \\ 0.778 \cdot e^{\left(\frac{T-80}{34.37}\right)} & T \geq 104 \text{ } ^\circ\text{C} \end{cases} \quad (6)$$

At 100 °C, water boils and induces lysis, causing necrosis and the loss of the physiological activity of cells. Equation 5 is applied under the hypothesis that the water steam does not leave the system, and that steam fills the tissue region at a lower temperature and condenses uniformly.

Constant values for the pancreas are $\rho = 1,040 \text{ kg m}^{-3}$, $c = 3,590 \text{ J kg}^{-1} \text{ K}^{-1}$, $k = 0.5417 \text{ W m}^{-1} \text{ K}^{-1}$, and $\lambda = 2,260,000 \text{ J kg}^{-1}$. Those for the quartz fibers are $\rho = 2,600 \text{ kg m}^{-3}$, $c = 820 \text{ J kg}^{-1} \text{ K}^{-1}$, and $k = 3 \text{ W m}^{-1} \text{ K}^{-1}$. Constants for the pancreas that are unavailable in the literature, e.g., c and the optical properties, are replaced with values for the liver [12, 13].

The theoretical prediction of the volume of ablated tissue is assessed as follows: where T reaches 100 °C, water in the cells of the pancreas vaporizes and tissue is ablated [14]. The volume in which this condition is met is indicated as V .

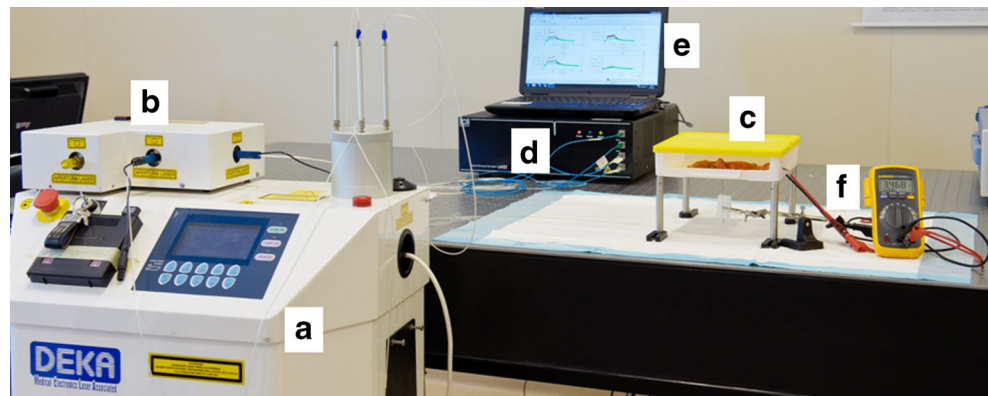
The theoretical study is implemented in COMSOL Multiphysics® 3.5a, considering a three-dimensional (3D) geometry in order to model the pancreas and the two applicators. The “Heat Transfer Module” has been used for the implementation of the Application Mode “Bioheat Equation” in transient analysis. The mesh is constituted of $33 \cdot 10^5$ tetrahedral elements, with a maximum size of 0.00099 m for the finest elements. The Linear System solver “Geometric Multigrid” was employed, with a computational time of 43,233 s. The initial tissue temperature and the boundary conditions are $T_0 = T_\infty = 310.15 \text{ K}$. Numerical simulations are performed considering both the heating and cooling phases.

Experimental assessment

Experimental trials are carried out to estimate both the temperature distribution around the two applicators and the ablated tissue volume.

The temperature distribution in two ex vivo pancreases undergoing LITT is monitored using the experimental setup illustrated in Fig. 2. The radiation of the Nd:YAG laser (Smart 1064, DEKA M.E.L.A. S.r.l., Florence, Italy, Fig. 2a) is split by its external beam splitter (Fig. 2b) into two beams of equal P (i.d., 3 W), which are then conveyed through the two applicators. The two applicators are guided inside the pancreases by means of a custom-made polymeric mask (Fig. 2c), employed to control the relative distances among the sensors and the laser tip applicators. The mask is also used to introduce four fibers (S_1 , S_2 , S_3 , and S_4), each one equipped with three-fiber Bragg grating sensors (G_1 , G_2 , and G_3 ; Technica SA, Zug, Switzerland), with lengths of 1 mm. The working principle of these

Fig. 2 Experimental setup for monitoring the temperature of ex vivo pancreases during LITT: (a) laser Nd:YAG, (b) beam splitter, (c) custom-made polymeric mask containing pancreatic tissue, (d) optical spectrum analyzer, (e) PC for data collection, and (f) NTC thermistor and multimeter



sensors is based on the phenomenon of radiation reflection; when light propagates through a fiber with a Bragg grating, a narrow range of wavelengths are reflected and the other wavelengths are transmitted. The so-called Bragg wavelength, λ_B , placed in the middle of the reflected range, can be expressed as:

$$\lambda_B = 2 \cdot n_{\text{eff}} \cdot \Lambda \quad (7)$$

with n_{eff} being the effective refractive index of the fiber core, and Λ the spatial period of the grating.

Since the temperature influences n_{eff} , the related change in λ_B can be considered an indirect temperature measurement [15], as expressed by the following relation:

$$\frac{\Delta\lambda_B}{\lambda_B} = c_T \cdot \Delta T \quad (8)$$

where $\Delta\lambda_B$ is the change in λ_B induced by temperature changes, ΔT , and c_T is the temperature coefficient.

$\Delta\lambda_B$ is detected by an Optical Spectrum Analyzer, OSA (Optical Sensing Interrogator, sm125, Micron Optics, Fig. 2d) with four channels, each of them connected to one fiber. To distinguish the output of each Bragg grating equipped in one fiber, they are characterized by three different λ_B , i.d., 1,533, 1,541, and 1,549 nm, at 23 °C. Experimental data acquired by the OSA, with a sampling frequency of 250 Hz, are sent to a PC (Fig. 2e). Finally, an NTC thermistor, with output picked up by a multimeter (Fluke 179, Digital Multimeter, Fig. 2f), is used to monitor the temperature of the pancreas before starting treatment (20 ± 1 °C).

Four 20-gauge needles and two 16-gauge needles are respectively used to insert the four fiber optics equipped with the FBG sensors and the two applicators into the pancreatic tissue. Sensors are positioned around the applicators in order to monitor the temperature because its distribution is a crucial factor in determining LITT outcomes. Figure 1a schematically reports their configuration. The four fiber optics (FO) with three FBG sensors (G) are set at four fixed distances from the two applicators A_1 and A_2 : FO_1 is placed between A_1 and A_2 at a distance of 2.0 mm, FO_2 is set equidistant from A_1 and A_2 at a distance of about 5.4 mm, FO_3 is placed at 8.0 mm from A_2 , and FO_4 is set equidistant

from the two applicators at a distance of about 15.1 mm. The centers of FO_1 , FO_2 , and FO_4 are aligned with each another, as are the centers of A_1 , A_2 , FO_1 , and FO_3 . Figure 1b represents the positions of the gratings within the same fiber, and their depth inside the pancreas. All G_1 of each fiber optic line are placed 2 mm upward from the A_1 and A_2 tips (Fig. 1b, black color), all G_2 are placed at the same level of the A_1 and A_2 tips (Fig. 1b, red color), and all G_3 are positioned 2 mm downward from the A_1 and A_2 tips (Fig. 1b, blue color).

In order to evaluate the volume of the lesion produced by LITT in an ex vivo pancreas, a magnetic resonance (MR) examination in the Radiology Department of our institution is performed. A 1.5-T MR (Siemens® Avanto, Erlangen Germany) is used, and the morphological sequences are applied immediately after treatment (about 3 min elapsed between the end of LITT and the beginning of the MR scan). Images of the pancreas just before the laser induction were also acquired in order to make a comparison.

Results

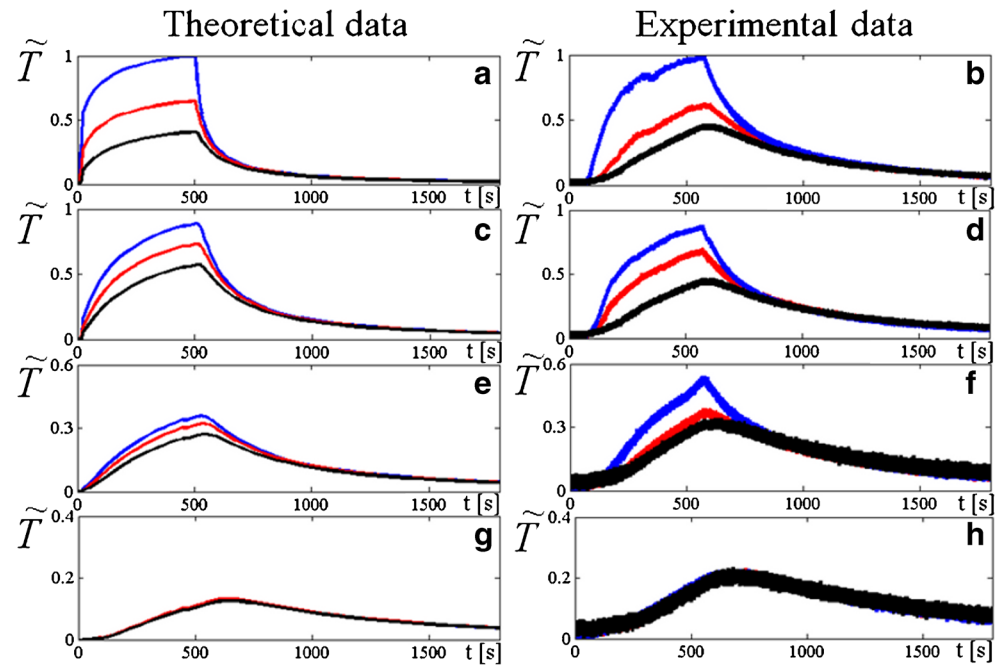
Numerical simulations, based on the theoretical model reported previously, are carried out in Comsol Multiphysics® environment with the aim to highlight the temperature distribution changes in the pancreas during the treatment (500 s) and during the subsequent cooling (between 500 and 1,800 s). Experimental trials are performed during LITT (500 s) and after stopping treatment (between 500 and 1,800 s) in order to monitor the temperature rise and tissue cooling phenomena in 12 sites around the applicators. Since the experimental tissue temperature is averaged on the whole FBGs length (i.e., 1 mm), the predicted temperature is calculated by averaging out the theoretical temperatures on 1 mm.

The adimensional parameter,

$$\tilde{T} = \frac{\Delta T}{\Delta T_{\text{max}}} \quad (9)$$

where ΔT is the temperature increase calculated in the four mentioned time points, and ΔT_{max} is the maximum ΔT

Fig. 3 Distribution of \tilde{T} in an ex vivo pancreas where the location of the FBG sensors correspond with the fiber positions FO₁, FO₂, FO₃, and FO₄: (a, c, e, g) theoretically predicted; (b, d, f, h) experimentally evaluated. Blue, red, and black lines, respectively, represent the temperature calculated 2 mm downward, at the same level, and 2 mm upward from the applicators



reached during the whole treatment between A₁ and A₂ (in correspondence of G₃ of the fiber FO₁; Fig. 1), is introduced.

Figure 3a, b, respectively, illustrates the theoretical and experimental trends of \tilde{T} within the pancreas in the regions where the FBG sensors are placed, during both the heating and cooling phases.

\tilde{T} obtained from temperatures measured during trials with FBG sensors placed around the applicator are reported in Fig. 3b.

Figure 4 shows the theoretical \tilde{T} distribution around the applicators at four time points: (1) when half the procedure

was completed at $t=250$ s (Fig. 4a); (2) at the end of the procedure, $t=t_L=500$ s (Fig. 4b); (3) during cooling, 250 s after the end of LITT, $t=750$ s (Fig. 4c); and (4) 600 s after the end of LITT, $t=1,100$ s (Fig. 4d).

Furthermore, both the theoretically predicted and experimentally assessed volumes of ablation in the pancreas undergone LITT are also estimated. The theoretical result of the ablated tissue volume, calculated as the volume of the region where T reaches 100 °C, is 0.95 cm³. This value agrees with the experimental value obtained by means of measurements

Fig. 4 Theoretical distribution of \tilde{T} in an ex vivo pancreas around the applicators: (a) 245 s after starting LITT and (b) at the end of the LITT; during the cooling phase: (c) 250 s after the laser treatment was stopped and (d) 600 s after the laser treatment was stopped

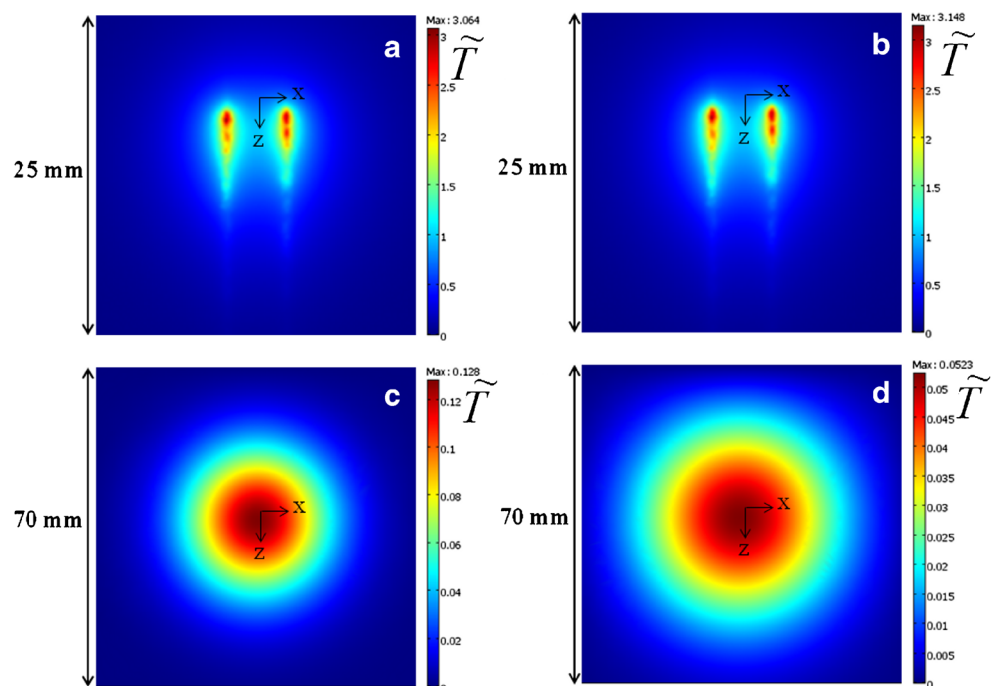
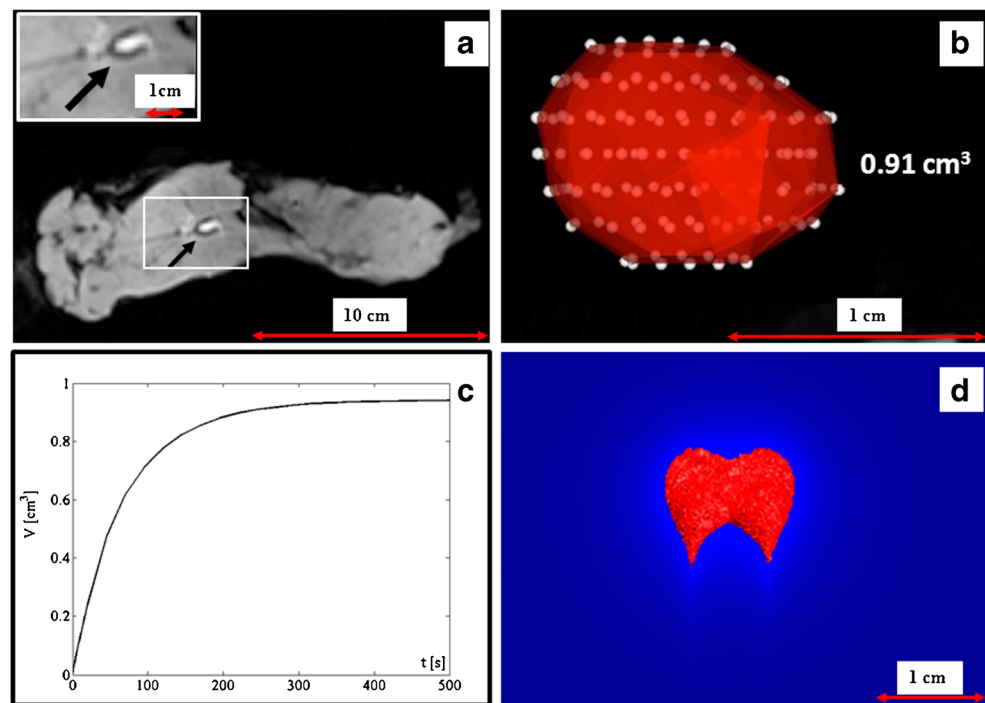


Fig. 5 MR image of the pancreas: (a) after laser treatment where the ablated tissue volume appears as a hypointense area, (b) 3D volume rendering post-processing reconstruction of the ablated tissue, (c) ablated volume as a function of treatment time obtained by the simulation, and (d) predicted ablated volume at the end of the treatment



based on MR images. In particular, the best results are obtained with T1-weighted gradient-echo (3D flash) sequences with fat saturation in the axial plane, where the lesion appeared as a hypointense area in the parenchyma with a thin peripheral hyperintense margin; to be sure that no artifacts influenced our analysis, the ablated cavity is filled with gadolinium (Dotarem Gadoteric Acid, Guerbet®, Ireland), a paramagnetic contrast agent commonly used in MR imaging which appears hyperintense in T1-weighted images (Fig. 5a).

A part of the pancreatic gland does not undergo significant morphological changes (Fig. 5a). The post-processing image software used to quantify the ablation is Osirix (Apple Inc.®, Cupertino, CA, USA); a 3D representation of the lesion is obtained, and the volume has been semi-automatically computed (Fig. 5b). The ablated volume as a function of treatment time obtained by simulation and the predicted ablated volume at the end of the procedure are shown in Fig. 5c, d, respectively.

The volume calculations by post-processing the images are repeated seven times in order to examine the repeatability of the method; the result is expressed as mean volume \pm the expanded uncertainty, $0.91 \pm 0.09 \text{ cm}^3$. The expanded uncertainty is estimated by multiplying the standard deviation of the seven measurements with a coverage factor of 2.45, which is obtained considering a Student's distribution with six degrees of freedom and a level of confidence of 95 % [16].

Discussion

During laser emission (up to $t=t_L=500 \text{ s}$), the heat deposition due to laser tissue interaction causes a marked temperature increase (ΔT) along the axes of the applicators. In fact, the highest value of temperature is reached immediately downward from the two applicators, as shown in Fig. 3a, b (FO_1 and FO_2). The maximum ΔT reached after 250 s is similar to the value at the end of the procedure (the difference is about 2.5 %, as shown by Fig. 4a, b). On the other hand, during cooling, the profile presents spherical symmetry because of the conductive heat exchange phenomenon, as shown in Fig. 4c, d. Approximately 250 s after the laser treatment is stopped, the hyperthermia has almost disappeared (temperature decreases to about 96 % of the maximum value), and at 1,100 s (i.d., 600 s after the laser treatment has stopped), the ΔT with respect to the initial temperature is less than 2 % of the maximum value reached at the end of the treatment.

The temperatures monitored closest to the applicators by sensors embedded in FO_1 confirm the theoretical results: (1) the highest temperature is measured at the end of the treatment by the grating placed downward from the applicators, as shown by the blue lines in Fig. 3a, b.

Table 1 Maximum temperature increase (ΔT_{max}) measured by each sensors during treatment

	FO ₁ ($d \approx 2 \text{ mm}$)			FO ₂ ($d \approx 5 \text{ mm}$)			FO ₃ ($d \approx 8 \text{ mm}$)			FO ₄ ($d \approx 15 \text{ mm}$)		
ΔT_{max} [°C]	G ₁	G ₂	G ₃	G ₁	G ₂	G ₃	G ₁	G ₂	G ₃	G ₁	G ₂	G ₃
	25	35	60	26	40	50	18	21	30	12	12	12

In order to make clear the comparison between our experimental data with results reported in literature, we illustrate the ΔT_{\max} measured by the 12 sensors in Table 1.

The maximum ΔT (ΔT_{\max}) measured by G_3 placed on FO_2 is 50 °C, showing a good agreement with the results presented in [17], where a ΔT of 60 °C is measured at 6 mm in porcine ex vivo tongue undergoing LITT. ΔT_{\max} also agrees with the results reported in [6] where a slightly lower value is obtained at a distance of 5 mm with similar laser settings and using one applicator. This underestimation could be related to the different length of the FBGs used in the two studies. FBGs with length of 10 mm are employed in [6]; therefore, the measured temperature are averaged out on 10 mm; indeed, the FBGs with length of 1 mm, employed in this study, allow to measure temperature with higher spatial resolution. This solution is particularly useful close to the applicator, where the thermal gradient is high. Moreover, in [17], ΔT values are of the same order of magnitude and decrease with increasing distances from the applicator. In the present study, values measured upward from the applicators (by G_1) are lower than the values measured by the grating placed at the same level of the applicators (i.d., G_2) during the entire trial; the maximum values reached by ΔT in the experiments are, respectively, 35 °C versus 25 °C. A further increase is observable in temperatures monitored downward from the applicators (by G_3). Furthermore, the trends obtained by the sensors placed on FO_2 , FO_3 , and FO_4 agree with the numerical results. The grating placed downward from the applicators measured higher temperatures (blue lines in Fig. 3b) than the grating placed upward from the applicators (black lines in Fig. 3b) as theoretically predicted (Fig. 3a). These differences increased when the distance from the applicators decreased. The good agreement is highlighted by the linear regression between the experimental maximum variation of temperature measured by the 12 FBGs during the treatment and the predicted ones. The correlation coefficient is 0.98, and the best fitting line is close to the line of equality (the slope was 0.996).

Concerning the temperature dynamics during laser treatment and during cooling, the higher the distance from the applicator, the higher the time required to reach the temperature maximum value and the time necessary to complete the cooling phenomenon. In order to clarify this concept, two examples are reported as follows: (1) during heating, the time necessary to reach $\Delta T_{\max}/2$ is about 90 s and about 110 s at distances of 2 and 5 mm from the applicators, respectively; (2) during cooling, the time necessary to reach $\Delta T_{\max}/2$ is about 150 versus 200 s, respectively, at distances of 2 and 5 mm from the applicators; a further increase is seen at measurements performed at a distance of 8 mm ($t \approx 300$ s). The increase of response time with the distance from the applicator is also reported in previous studies [6, 18].

Since several biological tissues (e.g., liver and prostate) strongly absorb Nd:YAG laser radiation ($\lambda=1,064$ nm), the ablation volume that can be achieved with the use of one optical fiber is limited and often is not sufficient for optimal treatment. Therefore, some authors introduced the technical solution of multiple applicator LITT in order to increase the lesion size by overlapping the lesions produced by each applicator [19, 20]. Experimental and theoretical results presented in this preliminary study and obtained with double-applicator LITT show a significant increase in the ablated pancreatic tissue volume, when compared with volumes described in [6] and performed with one fiber. This outcome is relevant, as far as it concerns both the increase in the lesion size and the reduction of treatment time. In fact, clinicians usually employ the pullback technique to increase the size of lesion, but the time required for each treatment increases; furthermore, the thermal effects obtained with the simultaneous use of two applicators are different than the thermal effects obtained with the successive use of two fibers. Finally, this modality aims to model the lesion shape by varying the distance between the applicators, according to the clinical necessities, as reported in [21]. This solution could allow to minimize the damage of extremely delicate structures surrounding the pancreas. Future work will focus on the evaluation of the influence of the distance between the applicators and the laser settings on the induced thermal effects.

Acknowledgments The authors would like to thank ITAL GM srl for the precious support provided.

Conflicts of interest The authors declare that they have no conflicts of interest.

References

1. Vogl TJ, Müller P, Weinhold N, Hummerstingl R, Mack MG, Böttcher H, Philipp C, Felix R (1995) MR-guided laser-induced thermotherapy (LITT) of liver metastases. In: Müller G, Roggan A (eds) Laser-induced interstitial thermotherapy. SPIE–The International Society for Optical Engineering, Washington
2. Whelan WM, Wyman DR (1999) Dynamic modeling of interstitial laser photocoagulation: implications for lesion formation in liver in vivo. *Laser Surg Med* 24:202–208
3. Saccomandi P, Schena E, Di Matteo FM, Pandolfi M, Martino M, Rea R, Silvestri S (2011) Laser interstitial thermotherapy for pancreatic tumor ablation: theoretical model and experimental validation. *Conf Proc IEEE Eng Med Biol Soc* 2011:5585–5588
4. Siegel R, Ward E, Brawley O, Jemal A (2011) Cancer statistics, 2011: the impact of eliminating socioeconomic and racial disparities on premature cancer deaths. *CA Cancer J Clin* 61:212–236
5. Winter J, Cameron JL, Campbell KA, Arnold MA, Chang DC, Coleman J, Hodgins MB, Sauter PK, Hruban RH, Riall TS (2006) 1423 Pancreaticoduodenectomies for pancreatic cancer: a single-institution experience. *J Gastrointest Surg* 10:1199–1211

6. Saccomandi P, Schena E, Caponero MA, Di Matteo FM, Martino M, Pandolfi M, Silvestri S (2012) Theoretical analysis and experimental evaluation of laser induced interstitial thermotherapy in ex vivo porcine pancreas. *IEEE Trans Biomed Eng* 59:2958–2964
7. Pennes HH (1948) Analysis of tissue and arterial blood temperature in the resting human forearm. *J Appl Physiol* 1:93–122
8. Niemz MH (2004) *Laser-tissue interactions: Fundamentals and application*, 3rd edn. Springer, Berlin, pp 15–18
9. Di Matteo FM et al (2012) US-guided Nd:YAG laser ablation in porcine pancreatic tissue: an ex vivo study and numerical simulation. Paper 1297200. Presented at the Digestive Disease Week, San Diego, 19–22 May 2012
10. Welch AJ, Van Gemert MJC (2011) *Optical-thermal response of laser-irradiated tissue*, 2nd edn. Springer, Berlin, pp 42–56
11. Yang D, Converse MC, Mahvi DM, Webster LG (2007) Expanding the bioheat equation to include tissue internal water evaporation during heating. *IEEE Trans Biomed Eng* 54:1382–1388
12. Müller G, Roggan A (1995) *Laser-induced interstitial thermotherapy*. SPIE Press, Bellingham
13. Gottschalk W (1992) Ein Meßverfahren zur Bestimmung der optischen Parameter biologischer Gewebe in vitro. Dissertation 93 HA 8984, Universität Fridericiana Karlsruhe, Karlsruhe
14. McKenzie AL (1990) Physics of thermal processes in laser-tissue interaction. *Phys Med Biol* 35:1175–1209
15. Rao YJ (2000) Fiber Bragg grating sensors: Principles and applications. In: Grattan KTW, Meggitt BT (eds) *Optical fiber and sensor technology: Fundamentals*. Kluwer Academic, Dordrecht, pp 355–380
16. BIPM (2008) Evaluation of measurement data—guide to the expression of uncertainty in measurement. *JCGM 100:2008*. BIPM, Sèvres
17. Ding Y, Chen N, Chen Z, Pang F, Zeng X, Wang T (2010) Dynamic temperature monitoring and control with fully distributed fiber Bragg grating sensor. *Proc SPIE* 7634:1–6
18. Lippert BM, Teymoortash A, Folz BJ, Werner JA (2003) Coagulation and temperature distribution in Nd:YAG interstitial laser thermotherapy: an in vivo animal study. *Lasers Med Sci* 18:19–24
19. Germer CT, Albrecht D, Roggan A, Isbert C, Burh HJ (1997) Experimental study of laparoscopic laser-induced thermotherapy for liver tumours. *Brit J Surg* 84:317–320
20. Veenendaal LM, de Jager A, Stapper G, Borel Rinkes IH, van Hillegersberg R (2006) Multiple fiber laser-induced thermotherapy for ablation of large intrahepatic tumors. *Photomed Laser Surg* 24:3–9
21. Heisterkamp J, van Hillegersberg R, Sinofsky EL, Ljzermans JNM (1999) Interstitial laser photocoagulation with four cylindrical diffusing fibre tips: importance of mutual fibre distance. *Lasers Med Sci* 14:216–220